Supplement of Atmos. Chem. Phys., 25, 3687–3715, 2025
https://doi.org/10.5194/acp-25-3687-2025-supplement

Atmospheric Chemistry and Physics
Open Access
EGU

Supplement of

In situ vertical observations of the layered structure of air pollution in a continental high-latitude urban boundary layer during winter

Roman Pohorsky et al.

Correspondence to: Roman Pohorsky (roman.pohorsky@epfl.ch) and Julia Schmale (julia.schmale@epfl.ch)

Supplementary material

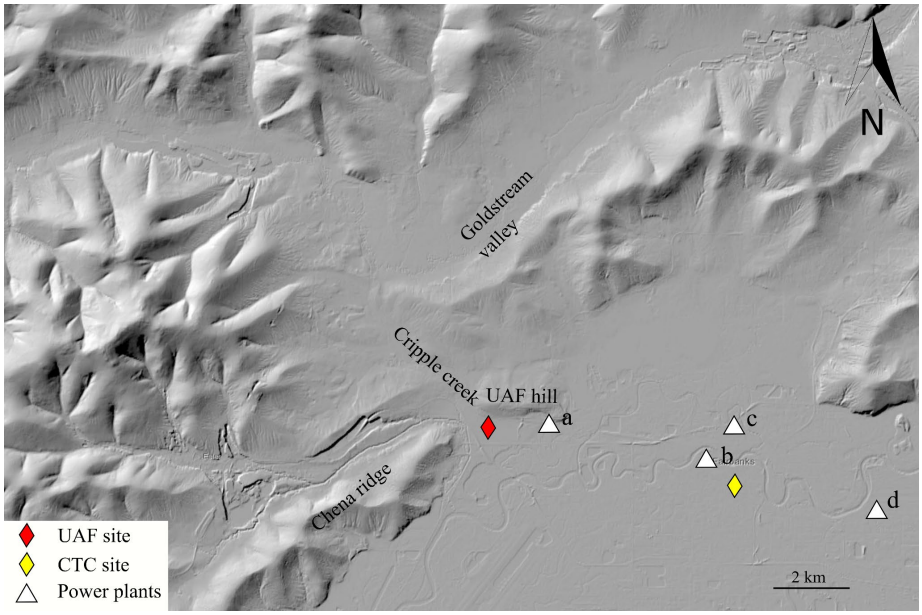

Figure S1 Topographic map of Fairbanks, Alaska, USA. The red and yellow diamonds represent the location of the UAF and CTC study sites, respectively. White triangles indicate the location of the power plants in Fairbanks. (a) UAF, (b) Aurora, (c) Zehnder and (d) Doyon (Fort Wainwright). The map was obtained and adapted from the United States Geological Survey (https://apps.nationalmap.gov/).

Table S1 List of flights. For the synoptic conditions, AC = anticyclonic and C = cyclonic. Instruments flown on specific flights are indicated by the following numbers: 1 = POPS, 2 = mSEMS, 3 = STAP, 4 = CO_2 monitor, 5 = CO monitor (Pico), 6 = O_3 monitor, 7 = MICROMEGAS multi gas sensor (see Table 1). A '-' in the last column indicates that no meteorological measurements are available for the flight.

Flight nr.	Date	Time	# of profiles	Maximum altitude	Instruments	Synoptic conditions	Temperature profile structure
1	2022-01-26	14:00 - 16:00	14	85	1, 4, 6,	AC	-
2	2022-01-27	23:00 - 00:20	4	290	1, 5, 6, 7	AC	Convex SBI[a]
3	2022-01-28	14:00 - 14:30	4	80	1, 3, 4, 6	AC	No SBI
4[d]	2022-01-30	6:00 - 10:40	8	350	1, 2, 4, 7	AC	Convex SBI

5	2022-01-31	14:00 - 16:00	10	85	1, 2, 3, 4, 7	AC	-
6[d]	2022-01-31	22:00 - 2:00	6	275	1, 2, 3, 4, 7	AC	Convex / S-shaped SBI
7[d]	2022-02-03	22:00 - 01:25	8	250	1, 3, 4, 5, 7	C	Convex SBI
8[d]	2022-02-04	02:00 - 03:05	4	180	1, 3, 4, 6, 7	C	Convex SBI
9[d]	2022-02-04	15:20 - 17:10	8	125	1, 3, 4, 5, 6	C	Convex SBI
10[c,d]	2022-02-06	22:50 - 00:30	2	225	1, 4	C	Convex SBI
11	2022-02-07	15:00 - 17:00	8	80	1, 2, 3, 4, 6, 7	C	No SBI
12	2022-02-08	22:00 - 01:00	8	250	1, 2, 3, 4, 7	C	No SBI
13	2022-02-09	01:00 - 03:00	4	330	1, 2, 3, 4, 7	C	No SBI
14[c]	2022-02-09	23:00 - 03:50	4	300	1, 4	C	Convex SBI[a]
15[d]	2022-02-10	17:00 - 19:00	10	140	1, 2, 3, 4, 5	C	Convex / S-shaped SBI
16[d]	2022-02-10	22:30 - 00:30	4	240	1, 2, 3, 4, 5, 7	C	S-shaped SBI
17	2022-02-19	15:00-17:00	8	110	1, 2, 3, 4, 5, 7	AC	Convex SBI / No SBI
18[c]	2022-02-19	21:30 - 03:30	2	280	4	AC	Convex SBI[b]
19[d]	2022-02-20	6:00 - 11:05	8	300	1, 2, 4, 7	AC	S-shaped SBI
20	2022-02-21	13:00 - 15:00	8	150	1, 2, 4, 7	AC	No SBI
21	2022-02-22	22:00 - 03:00	2	300	1, 4	C	Convex SBI
22	2022-02-23	13:00 - 15:00	8	125	1, 2, 4, 5, 6, 7	C	-
23[c,d]	2022-02-23	21:30 - 03:00	2	300	1, 4	C	S-shaped SBI
24[d]	2022-02-25	09:50 - 12:40	4	175	1, 2, 4, 6, 7	C	Convex SBI

[a]The SBI was not observed on all profiles due to either a SBI erosion or SBI formation during in between profiles.

[b]Instrument issue during the flight

[c]Flights with an instrumental payload for aerosol filter sampling for chemical analysis (details not discussed here, see Pohorsky et al., 2024 for details)

[d]Flights used for the analysis of the mixing layer height and temperature inversion profile (Table 2).

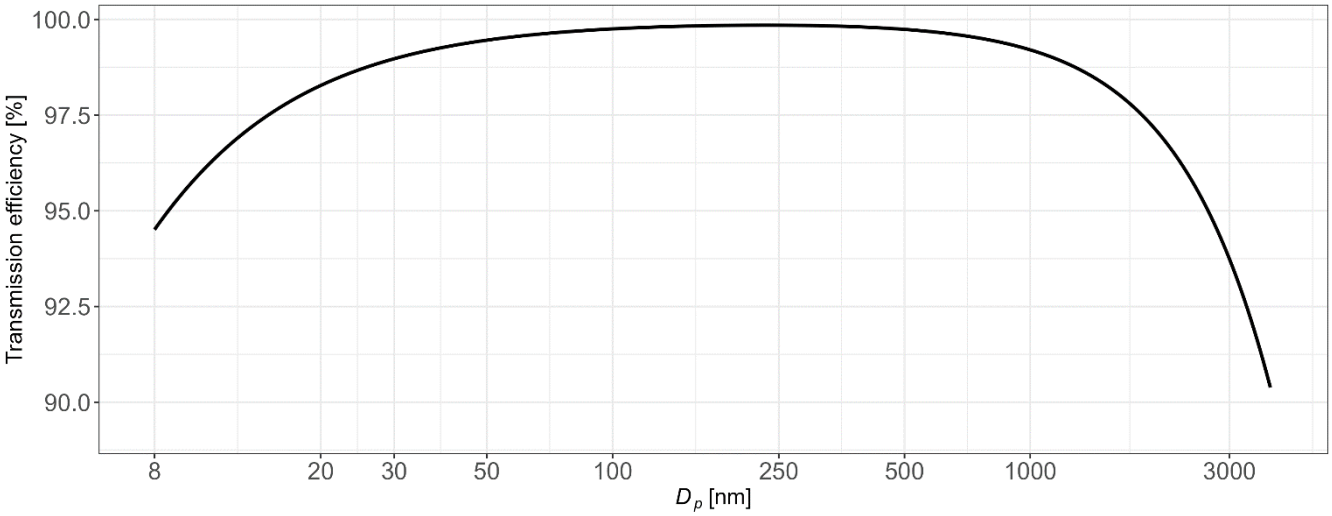

Figure S2 Particle transmission efficiency for the inlet used for ground-based measurements. The transmission efficiency was calculated using the Particle Loss Calculator (PLC) (von der Weiden et al., 2009) and is expressed in percent of the particles transmitted through the inlet as a function of particle diameter D_p (nm).

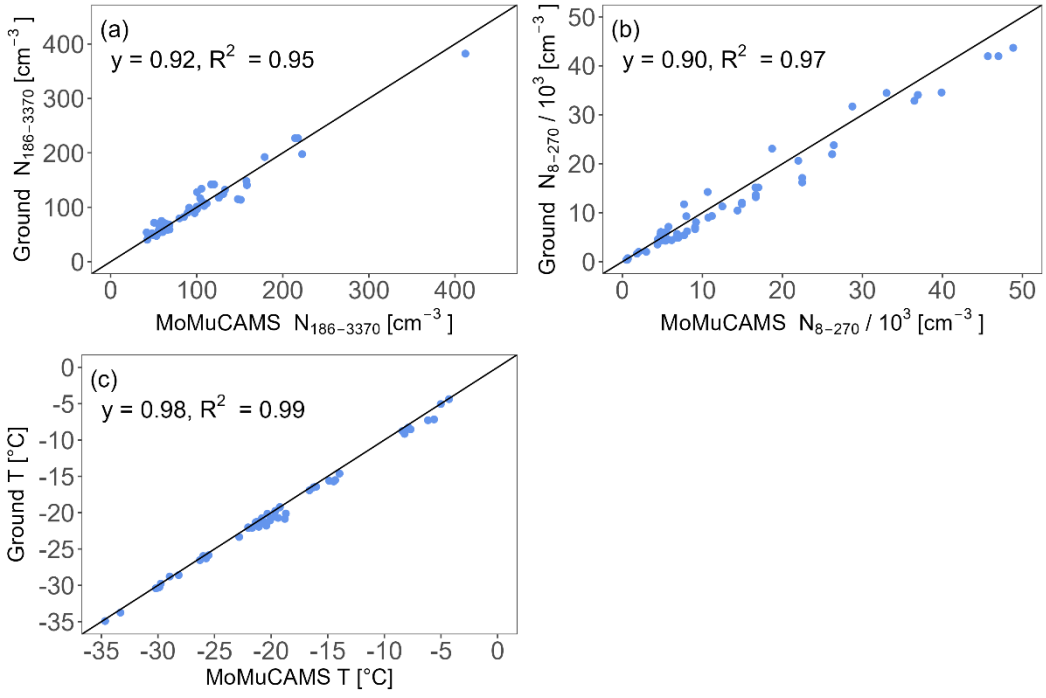

Figure S3 Scatterplots of MoMuCAMS measurements in the lowest 2 m of each profile (average) and corresponding ground-based measurements for (a) $N_{186-3370}$, (b) N_{8-270} (cm^{-3}) and (c) temperature (°C). The black diagonal represents the 1:1 line. The regression slope of a linear fit and the coefficients of determination (R^2) are indicated in each panel.

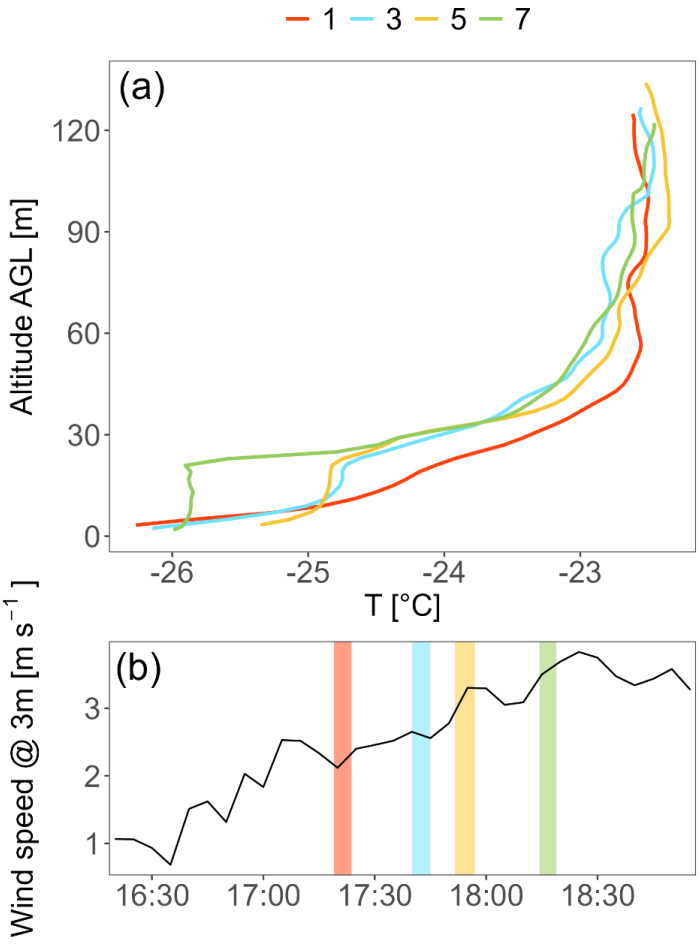

Figure S4 (a) Temperature profiles on February 10, 2022 (Flight 15) and (b) wind speed at 3 m. The colour of the profiles and of the shaded rectangles represent the profile numbers of the flight.

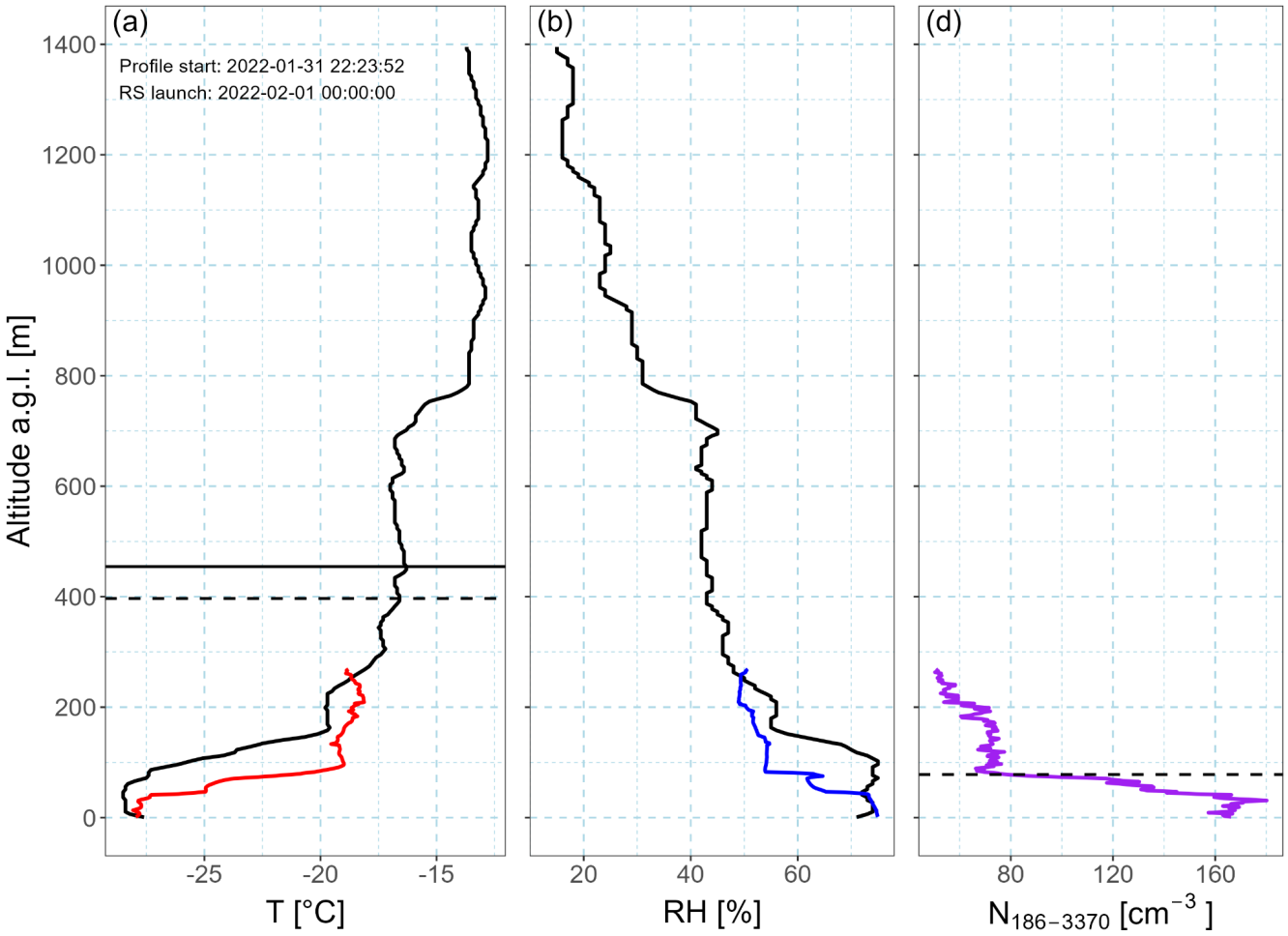

Figure S5 (a) Temperature profiles measured by a radiosonde (RS) at the Fairbanks airport (PAFA) on February 1st at 00:00 LT (black profile) and by the Helikite on January 31st at 22:24 LT (red profile). The horizontal full (dashed) line indicates the top of the SBI identified with a 0 °C / 100 m (0.65 °C / 100 m) threshold. (b) Relative humidity profiles from the radiosonde (black) and Helikite (blue). (c) $N_{186\text{-}3370}$ profile. The horizontal dashed line indicates the top of the mixing layer (h_{mix}).

Comparison of h_{mix} to parameterizations of the stable boundary layer height

The analysis presented in Sect. 4.1 provides a direct answer to the question of the vertical extent of the mixing of surface pollution emissions at the study site during the campaign. However, it does not represent a practical method for operational purposes, given the logistics of tethered-balloon operations. A common method to assess the stable boundary layer height (SBLH) are surface measurements of turbulent fluxes (Vickers and Mahrt, 2004). Since our measurements do not assess the turbulence profile but rather the effect of mechanical mixing on pollutants, we are interested to know if our observations of the surface pollution mixing layer correspond to flat-terrain formulations of the SBLH. This comparison is made under the assumption that the vertical extent of the SBL agrees with the vertical extent of the pollution mixing layer, which is not necessarily the case according to Seibert et al. (2000). Such formulations offer however, the advantage that surface flux measurements can be continuously acquired to obtain a diagnostic of the SBLH. We select four different formulations and compare them to our observations. For the comparison, we choose a very simple formulation proposed by Koracin and Berkowicz (1988) (h_{KB}) and three more complex formulations from Zilitinkevich and Baklanov (2002) (h_{ZB}) and from Steeneveld et al. (2007) (h_{S1} & h_{S2}). The h_{KB} formulation was selected for its simplicity as it only requires the friction velocity and location to compute the Coriolis parameter. The other formulations were chosen because they represent work specifically adapted for very stable boundary layers. The equations are listed in Table S2.

Table S2 List of diagnostic equations for the stable boundary layer height. N is the free flow stability parameter (Brunt-Vaisala frequency), u_* is the friction velocity, L is the Obukhov length, $|B_s|$ is the buoyancy flux and f is the Coriolis parameter. $C_R = 0.4$, $C_{UN} = 0.25$ and $C_S = 0.75$ are dimensionless empirical constants. $\lambda = [C_1 - 0.001(N/f)]^{-1}$ and $C_1 = 1.8$.

Variable	Definition	Reference	Original equation number in reference
h_{KB}	$h_{KB} = \frac{0.07u_*}{f}$	Koracin and Berkowicz (1988)	Eq. 7
h_{ZB}	$h_{ZB} = \frac{C_R u_*}{\|f\|}\left[1 + \frac{C_R^2 u_*(1+C_{uN}NL/u_*)}{C_S^2 \|f\|L}\right]^{-1/2}$	Zilitinkevich and Baklanov (2002)	Eq. 11
h_{S1}	$h_{S1} = L\left(\frac{\left\|\frac{g}{\theta}\overline{w\theta_s}\right\|}{\alpha u_* fNL}\right)^{\lambda}$	Steeneveld et al. (2007)	Eq. 3
h_{S2}	$h_{S2} = \{10u_*/N \ for \ u_*^2N/\|B_s\| > 10 \ 32(\|B_s\|/N^3)^{1/2} \ for \ u_*^2N/\|B_s\| < 10$	Steeneveld et al. (2007)	Eq. 4

Figure S6 shows results of the comparison between the observed h_{mix} and the different formulations. Colors indicate whether the SBI has a convex structure (red) or a 's-shaped' structure (blue). To maximize the number of data points, h_{mix} from individual profiles was used. For calculation of the SBLH from equations in Table S2, the last flux parameters calculated from the eddy covariance tower (c.f. Sect. 2.2.2) before the start of the vertical profile measurements were used. Ranges of u_*, L,

$|B_s|$, N and heat flux (H) measured before the profiles are listed in Table S4. The calculated roughness length at the site equals 0.006 m. Since the eddy covariance tower was removed on February 17th and because temperature data were not recorded for some of the initial flights, only 29 profiles (from 7 flights) were used for the comparison. Table S3 shows metrics of the models' performance. Overall, h_{KB} demonstrates the lowest performance (Pearson correlation r = 0.16) and h_{S1} performs the best (r = 0.50). The Pearson correlation for h_{S2} and h_{ZB} is 0.4 and 0.25, respectively. Generally, all models have a negative bias and large root mean squared error (RMSE) in comparison to our derived h_{mix}. This bias could be related to the type of comparison between an observed pollution mixing layer height and diagnostic formulations of the SBLH. Since the stable boundary layer is known for intermittent turbulence bursts (Salmond and McKendry, 2005), this could lead to a higher extent of the surface pollution.

To understand what might have caused these discrepancies, we compared the measured flux parameters at the UAF farm site with those from Steenveld et al. (2007) at the SHEBBA station (drifting station in the pack ice north of Alaska, from approximately 75 °N, 144 °W to 80 °N, 166 °W), which represents a more similar surface to the UAF farm site (compared to other sites from the Steeneveld et al. (2007) study).

The typical u_* values calculated during flights were between 0.031 and 0.163 m s^{-1}, while Steeneveld et al. (2007) observations ranged from 0.1 to 0.22 m s^{-1}. H at the UAF farm ranged from -5.7 to -0.1 W m^{-2} and from -18.0 to -6.7 W m^{-2} at the SHEBBA station. These lower values at the UAF farm site could explain the diagnosed low altitude of the SBLH. This seems to be particularly the case for H, which typically becomes very low under very stable boundary layer conditions as static stability suppresses turbulence (Wiel et al., 2012). This phenomenon has also been previously reported by Maillard et al. (2022) at the UAF farm site under low wind conditions. Overall, these lower turbulence parameter values indicate that the observed stability of the atmosphere at the UAF farm is more pronounced than over sea ice north of Alaska (likely because of lower wind speeds in Fairbanks) and might represent a limit to the tested formulations. We also observe that under cases of 's-shaped' SBI, which are associated with higher wind speeds and increased surface turbulence, all models perform better. The Pearson correlation increases from 0.16 to 0.26 for h_{KB} and from 0.5 to 0.73 for h_{S1}. However, despite showing the best performance, the root mean square error of h_{S1} for cases of 's-shaped' SBIs represents almost 30% of the mean observed mixing layer height with a mean bias of 15.7 m.

A more in depth analysis of available models and reconciliation with observations is beyond the scope of this paper. We can conclude however, that h_{S1} seems to perform the best, while h_{KB} shows the poorest performance for the extremely stable conditions of the high latitude winter boundary layer. All models perform better under higher wind speed conditions, when stronger turbulence occurred. However, generally, the relatively large biases and RMSEs are non-negligible. Given the very low h_{mix} at the UAF farm site, errors in predicting the height will lead to substantially different estimates of mixing layer heights and, consequently, pollution concentrations.

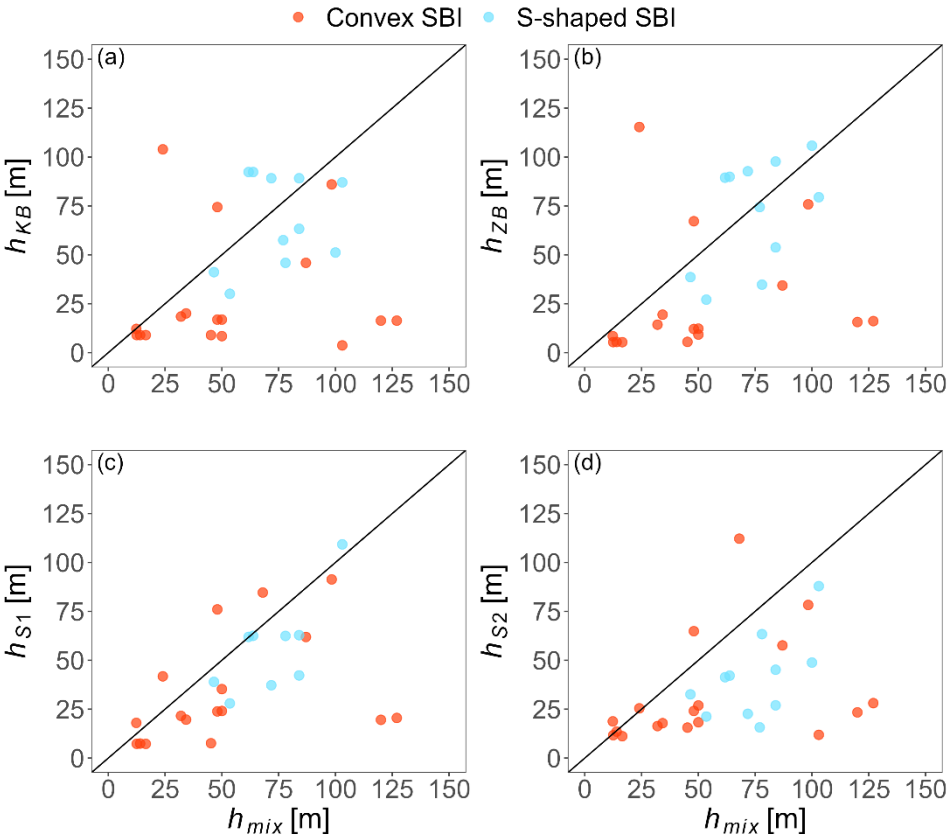

Figure S6 Comparison of observed mixing layer height (h_{mix}) and different surface flux-based formulations of the boundary layer height. Red points represent cases where the SBI has a convex structure. Blue points represent cases of 's-shaped' SBIs. The black diagonal represents the 1:1 line.

Table S3 Model performance statistics. Results are shown for the overall comparison and for cases of convex and 's-shaped' SBI. The n indicates the number of data points used for the comparison, MB is the mean bias, RMSE is the root mean squared error and r is the Pearson correlation coefficient.

model	SBI type	n	MB (m)	RMSE (m)	r
H_{KB}	all	29	-9.0	66.1	0.16
H_{ZB}	all	28	-7.1	61.2	0.25
H_{S1}	all	26	-17.7	34.7	0.50
H_{S2}	all	29	-27.2	41.8	0.40
H_{KB}	Convex	18	4.9	104.0	0.11
H_{ZB}	Convex	17	-9.4	76.2	0.15
H_{S1}	Convex	17	-18.8	39.8	0.40
H_{S2}	Convex	18	-23.0	43.8	0.34
H_{KB}	'S-shaped'	11	14.3	33.3	0.26
H_{ZB}	'S-shaped'	11	-3.6	23.8	0.49
H_{S1}	'S-shaped'	9	-15.7	22.0	0.73
H_{S2}	'S-shaped'	11	-34.1	38.3	0.57

Table S4 Ranges of surface flux parameters used for the calculation of the stable boundary layer height in Sect. 4.2

	25th	50th	75th
u_* [m s^{-1}]	0.031	0.078	0.163
L	0.26	3.8	17
H [W m^{-2}]	-5.7	-0.9	-0.1
$\lvert B_s \rvert$	-2.26 x 10^{-4}	-4.51 x 10^{-5}	-1.9 x 10^{-5}
N [Hz]	0.039	0.042	0.045

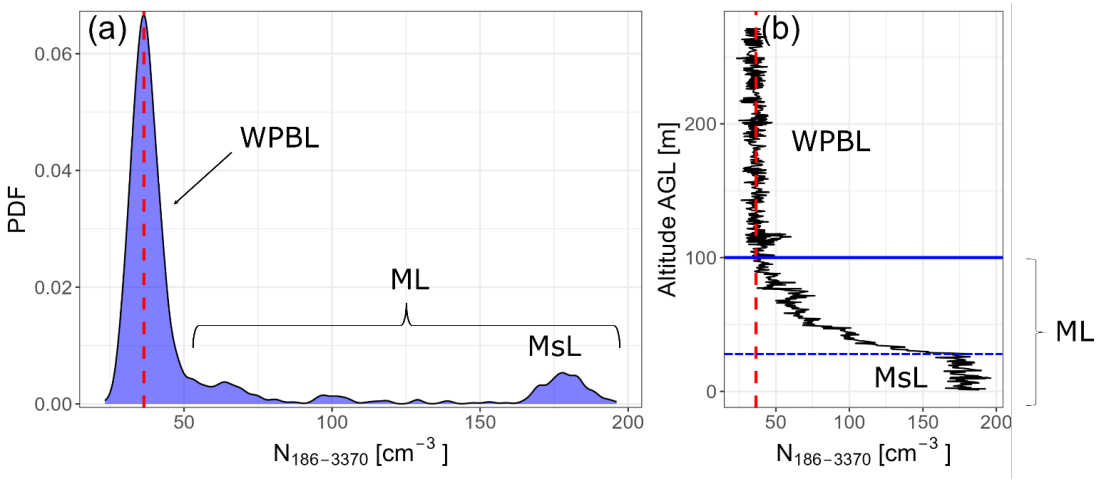

Figure S7 (a) Probability density function of the particle number concentration from 186 to 3370 nm ($N_{186-3370}$) in a vertical profile on January 27. The mode on the left represents the WPBL. The vertical red dashed line is the average of the WPBL distribution used as a background value for the concentration differences calculated in Sect. 5. (b) Vertical profile of $N_{186-3370}$. The red dashed line is the WPBL average concentration. The horizontal blue dashed and full lines represent the height of the MsL and ML respectively.

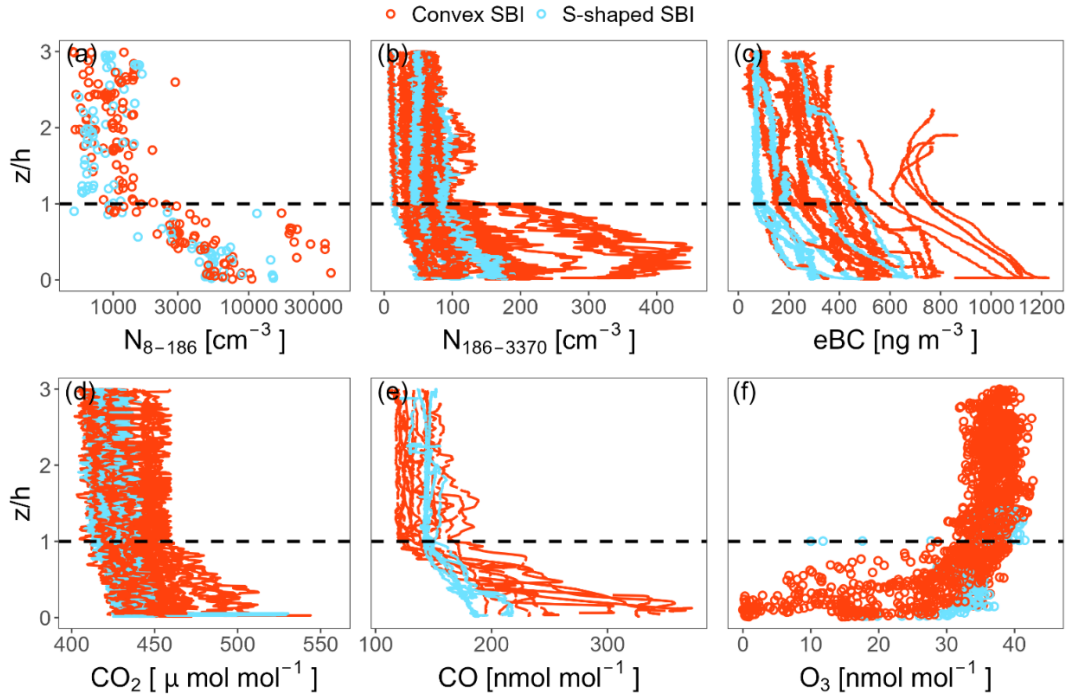

Figure S8 Vertically normalized profiles. (a) N_{8-186}, (b) $N_{186-3370}$, (c) eBC (d) CO_2 mixing ratio, (e) CO mixing ratio and (f) O_3 mixing ratio. The altitude (z) is normalized by the observed stable boundary layer height (h_{mix}). The profiles correspond to those in Fig. 11 but in absolute values. Profiles are color-coded based on the SBI type.

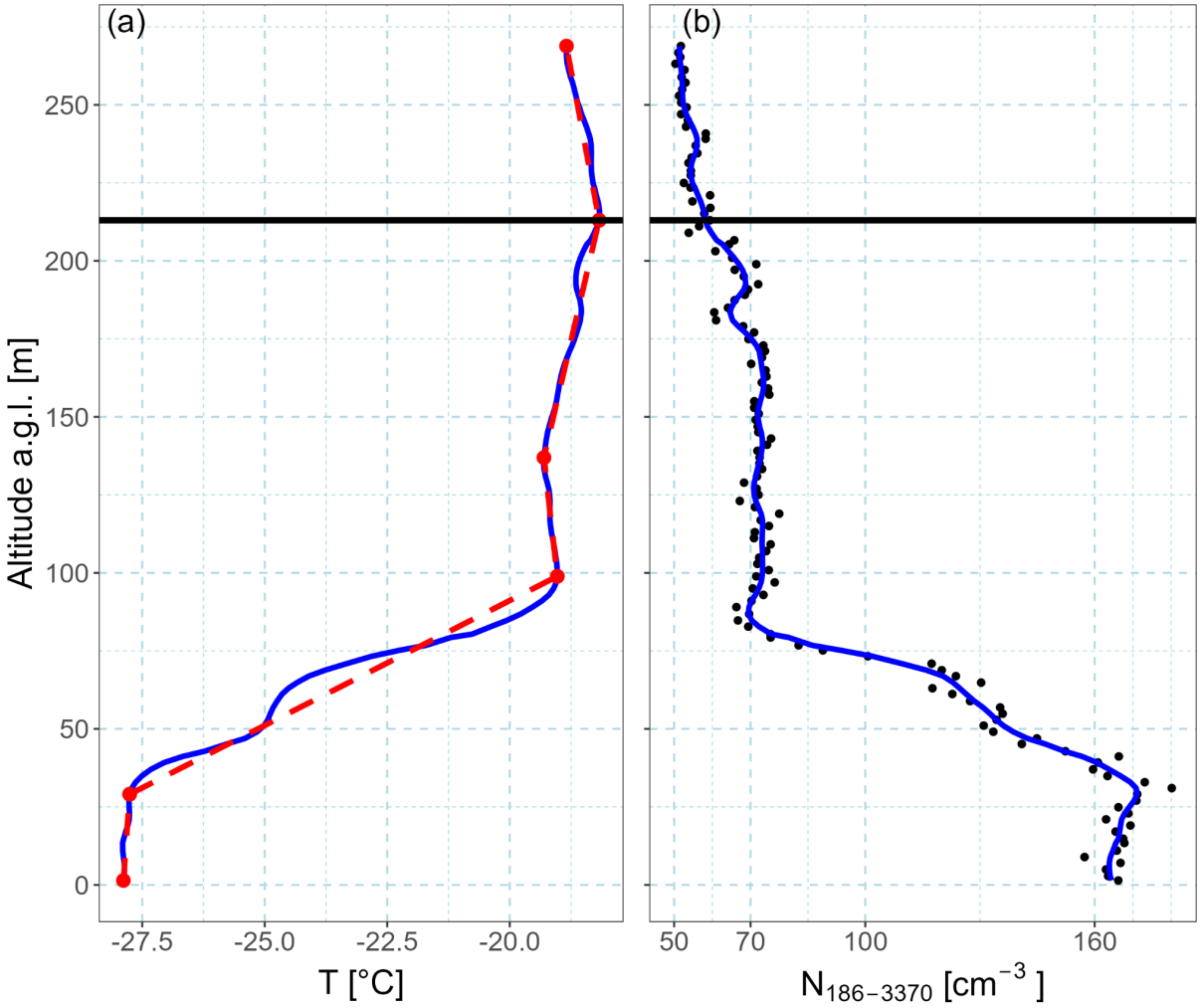

Figure S9 (a) Temperature profile on January 31 at 22:20 LT. The blue line represents the measured temperature with a gaussian smoothing over 20 meters. The red line represents the temperature profile from the temperature layering analysis (c.f. Sect. 2.3). (b) $N_{186-3370}$ profile. The black dots represent the 2-m averaged profile. The blue line represents the gaussian smoothed profile. The horizontal black line marks the top of an EI and the lower limit of the FTBL.

Comparison of pollution levels in the LBL and WPBL to reported Arctic haze background values

Table S5 indicates median (and interquartile range) values of the various measured tracers during ALPACA in the different layers and situations discussed in Sect. 4 and 5. The last column of Table S5 shows Arctic haze background values for submicron particle number concentrations from the literature. Background values represent either free tropospheric haze values or surface high latitude haze values for same period of the year (January – February) if available.

In April 2008, during the Aerosol, Radiation, and Cloud Processes affecting Arctic Climate (ARCPAC) project an aircraft measured the free tropospheric background haze concentrations above north Alaska (Brock et al., 2011). Six flights were carried out from April 11 to April 21, 2008 from Fairbanks. The aircraft was equipped with various aerosol and trace gas instruments. The flight region covered the northern part of Alaska and sea ice to the north. Flights included profiles up to 7400 m in altitude and down to 70 m. Four different air masses were intercepted during those flights, and classified according to the gas-phase composition of the air. Out of those four air masses, a free tropospheric haze background layer was identified and characterized by sulfate-rich aerosol extending from the top a surface-based inversion over sea ice to an altitude of 7400 m. Here, we used reported values of aerosol number concentration, CO and O_3 mixing ratios from Brock et al. (2011). Additional comparison of eBC values was made with data from Schmale et al. (2022) who analyzed seasonal cycles and trends of aerosol properties at 10 Pan-Arctic stations and Boyer et al. (2023) who compared Arctic station's aerosol measurements to aerosol data collected during the MOSAIC expedition. We used their data from Utqiagvik/Barrow for the months of January and February from 1992 to 2019. We also compared our observation to vertical measurements from Mazzola et al. (2016), Ferrero et al. (2016) and Cappelletti et al. (2022) who performed tethered-balloon measurements over Ny-Ålesund, collecting vertical profiles of eBC concentrations.

Freud et al., (2017) analyzed the seasonality and transport patterns driving aerosol number size distribution from 20 to 500 nm across several Pan-Arctic stations from 2007 to 2015 (Alert, Villum Research Station – Station Nord, Zeppelin, Tiksi and Utqiagvik/Barrow). We used results at Utqiagvik/Barrow during January/February to compare with the LBL values from the Helikite flights. Although the measurements from Freud et al. (2017) were taken at the surface, they constitute a useful reference for Arctic haze values for the North American sector of the Arctic. We also compared our PNSD to their haze size distribution identified from a k-means clustering analysis from the Alert, Villum - Station Nord and Zeppelin stations. This comparison is made under the assumption that the average Arctic haze PNSD are homogenous throughout the Arctic. Finally, we used reported values from Engvall et al. (2008) who reported PNSD from 20 to 630 nm from the Zeppelin station for the month of April between 2000 and 2005.

Kinase et al., (2023) analyzed CO measurements from 2016 to 2020 at the Poker flat research range located 30 km north of Fairbanks. This dataset constitutes background boundary layer values for northern Alaska. Given its geographical proximity to Fairbanks, this data constitutes a good regional background reference as it is not directly influenced by fresh pollution emissions, yet close to Fairbanks. Finally, Whaley et al. (2023) reported the seasonality of CO and O_3 mixing ratios, including at Utqiagvik/Barrow and vertical profiles from observations and modelling studies. We used their observations for the months of January and February for comparison.

Table S5 Table of concentrations and mixing ratios measured in the different layers and under various situations by the Helikite during ALPACA. The first value always indicates the median and the values in brackets represent the 25th and 75th percentile, respectively. Background values in the last column refer to measurements of submicron particle number concentrations in Arctic haze at various elevations.

	MsL (Convex SBI)	MsL (s-shaped SBI)	No SBI flights	WPBL (easterly wind)	WPBL (other wind direction)	LBL	Literature reported background values
$N_{8\text{-}186}$ [cm^{-3}]	6000 (4500 - 8490)	5430 (5160-6860)	1000 (800-3600)	1220 (820 - 1480)	670 (310 - 890)	174 (149-215)	371* (Brock et al., 2011) 200 – 250** (Freud et al., 2017)
$N_{186\text{-}3370}$ [cm^{-3}]	112 (85-182)	98 (88-110)	55 (53 - 57)	56 (47 - 65)	49 (40 - 58)	45 (42 - 50)	
eBC [ng m^{-3}]	550 (500 - 700)	290 (260 - 490)	126 (112-142)	230 (180 - 290)	80 (65 - 130)	56 (52-74)	60 (Brock et al., 2011) 58 [31 - 103] (Schmale et al., 2022)
CO_2 [µmol mol^{-1}]	443 (435 - 458)	436 (432 - 441)	426 (423-435)	423 (416 - 433)	420 (416 - 424)	420 (418 - 422)	-
CO [nmol mol^{-1}]	237 (200 - 255)	185 (182 - 209)	-	132 (121 - 140)	143 (135 - 148)	-	161 ± 8 (Brock et al., 2011) 131 (107 - 150) (Kinase et al., 2023) ~ 140 – 150 (Whaley et al., 2023)
O_3 [nmol mol^{-1}]	16 (6 - 26)	30 (27 - 31)	33 (31 - 34)	38 (36 - 39)	38 (37 - 39)	-	52 ± 14 (Brock et al., 2011) 32 - 35 (Whaley et al., 2023)

*Size range: < 1000 nm

**Size range: 20 – 500 nm

***Size range: 20 – 630 nm

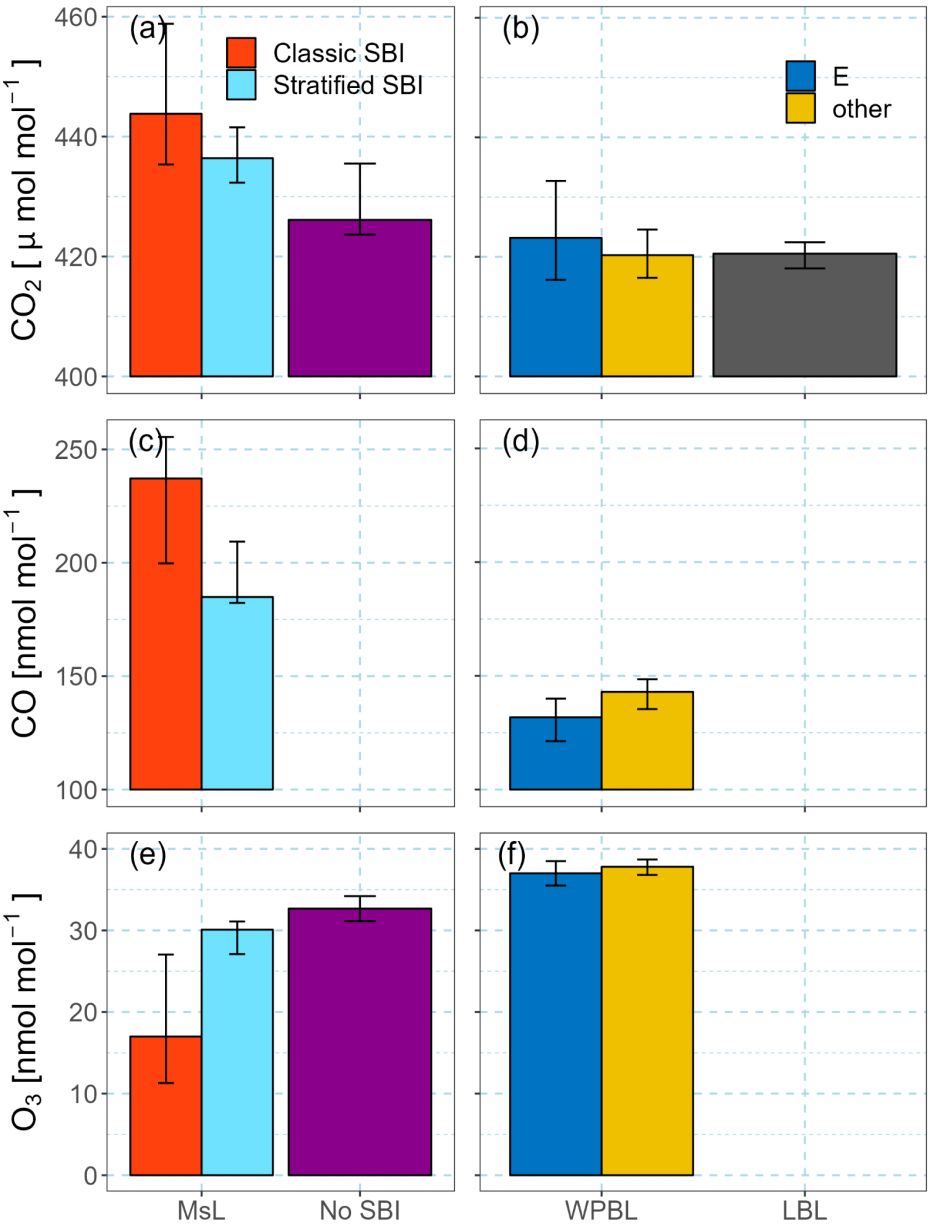

Figure S10 Median mixing ratios of CO_2 (a and b), CO (c and d) and O_3 (e and f). Left panels show values in the mixed sublayer (MsL) under conditions of convex SBI (red) and 's-shaped' SBI (blue) and without an SBI (purple). Right panels show values in the WPBL under different dominant wind directions (blue and yellow) and in the LBL (grey). The error bars indicate the interquartile range. If a bar is not shown, it means that no measurements of the specific tracer are available for the specific layer or situation.

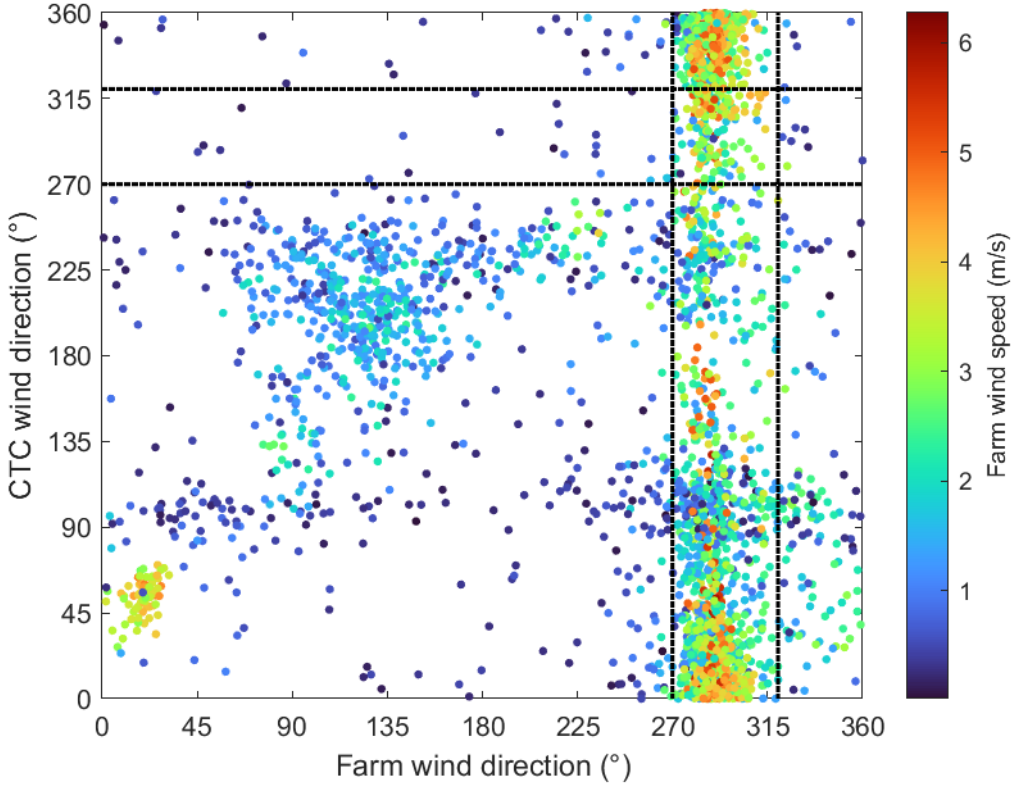

205

206 **Figure S11 Wind speed and direction measured simultaneously at the UAF farm and CTC sites during the ALPACA campaign. The**
207 **dashed lines indicate the direction range associated with the SCF. Dots that fall inside this range at both sites indicate that the SCF**
208 **was also measured at CTC.**

209

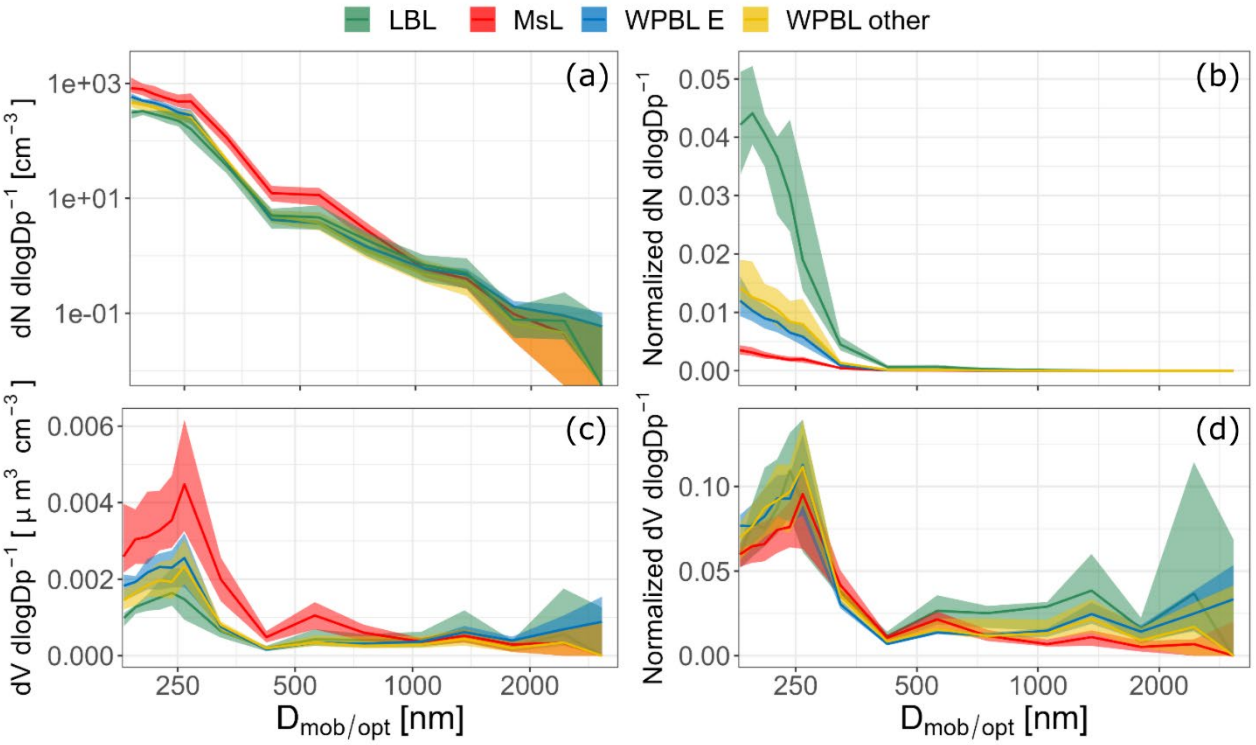

Figure S12 (a) Particle number size distribution in the mixed sub-layer (red), in the weakly polluted background layer under easterly dominant winds (blue) and other wind directions (yellow) and above the EIs in the lowest background layer (green). (b) Normalized PNSD in the same layers. (c) PVSD in the same layers. (d) Normalized PVSD in the same layers. The displayed size range is from 180 to 3370 nm and is merged from the mSEMS and the POPS.

Table S6 Particle number size distribution fit parameters from Fig. 11. The μ is the mode diameter and σ is the standard deviation of each respective mode.

Layer	μ [nm]	σ [nm]	mode
MsL	28.8 ± 1.8	22.1	Aitken
	181 ± 1.4	86.2	Accumulation
WPBL (Easterly wind)	26 ± 1.7	34.1	Aitken
	182 ± 1.4	87.2	Accumulation
WPBL (other)	32.6 ± 2.1	35.5	Aitken
	187 ± 6.0	100.5	Accumulation
LBL	32.7 ± 2.1	124	Aitken
	193.1 ± 6.7	90.8	Accumulation

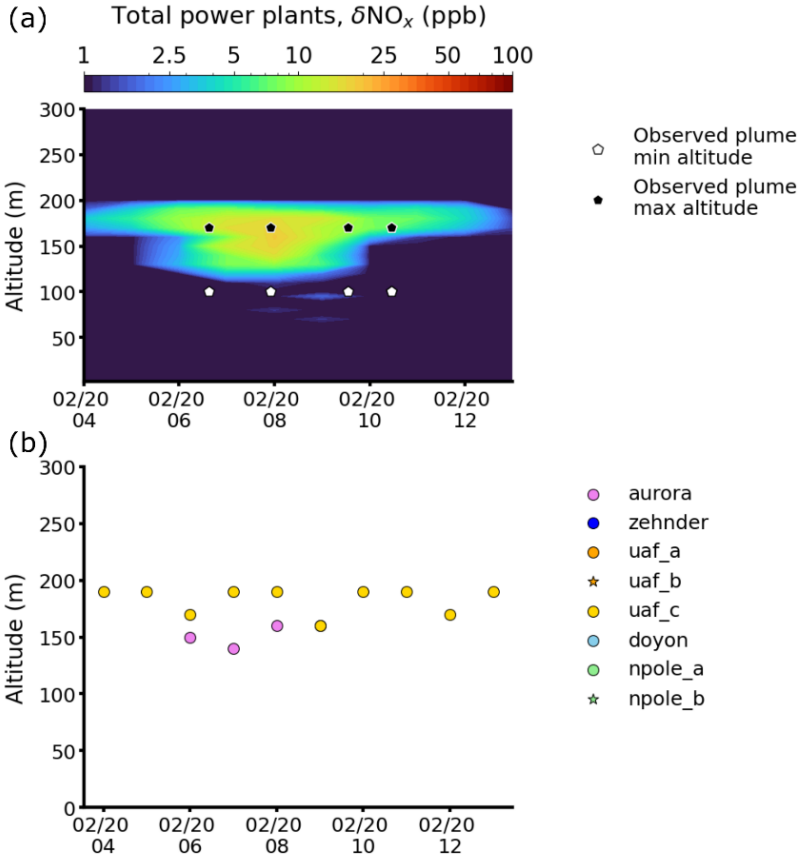

Figure S13 Figure S6: (a) Timeseries of the vertical distribution of simulated NO_x tracer enhancements above background (ppb) from the different power plants in Fairbanks for the 1.33 x 1.33 km grid box covering the UAF site from 0400 to 1400 AKST on 20 February 2022. (b) Altitudes of the different power plant plumes simulated over the UAF site for the same period. Results are from FLEXPART-WRF pollution dispersion model simulations for the ALPACA-2022 campaign. See Brett et al. (2024) for details.

Table S7 List of power plants in Fairbanks with the respective fuel type and stack height

Power plant	Fuel type	Stack height [m]
UAF A	Diesel	20
UAF B	Diesel	20
UAF C	Coal	64
Aurora	Coal	48
Zehnder	Diesel	18
Doyon	Coal	26

Plume identification details:

For the analysis presented in Sect. 6.2, the edges of each plume were determined visually where the profile of various tracers marked a sharp inflection point. In some flights, three different plume layers were identified. Enhancement factors inside the plume were derived as described in Sect. 6.1 (with regard to the WPBL). The measured vertical profiles were compared to the simulated FLEXPART-WRF tracer enhancements and wind directions from the wind LiDAR at plume height to identify the most likely source of the plumes. Four plumes were attributed to the UAF C power plant. The observed height of the plumes from UAF C ranged from 90 to 290 m. The other plumes were observed at heights between 50 and 277 m. The specific sources of these other plumes are however less certain as the model either did not predict any plume at the specific observed height or the simulated plume signal was weak and/or slightly displaced horizontally from our observations (see Brett et al. (2024) for discussion about model performance). The potential sources attributed to these plumes included the UAF A, B and C, Aurora, Doyon and Zehnder power plants. In a few cases, no potential sources were readily identified by the model. Table S8 lists the different identified plumes with their attributed potential source. Table S7 lists the different power plants from the Fairbanks area with associated fuel types and stack heights. Their location is indicated in Fig. 1.

Table S8 List of analyzed plumes with their respective potential source. Shaded rows are plumes with insufficient data for the tracer-tracer relationship analysis. A question mark indicates an alternative unknown source. In certain situations, several potential sources are indicated.

Plume ID	Flight #	Profile date & time	Average plume center height	source
11*	1	2022-01-26 15:47 – 16:02	54	? / UAF A & B[a]
51	4	2022-01-30 07:42 – 08:23	206	?
52	4	2022-01-30 07:42 – 08:23	160	? / Aurora[a]
53	4	2022-01-30 06:43 – 08:23	33	? / UAF A&B[a] / Doyon[a] / Aurora[a]
91	7 & 8	2022-02-04 01:04 – 02:57	110	UAF C
141**	13	2022-02-09 01:25 – 03:02	277	? / UAF C[a] / Zehnder[a]
142**	13	2022-02-09 01:25 – 03:02	244	UAF C
191*	18	2022-02-20 03:18	160	UAF C
201	19	2022-02-20 06:37 – 10:26	148	UAF C
202	19	2022-02-20 06:37 – 10:26	148	UAF C
231***	22	2022-02-23 13:01 – 13:15	50	? / Chena ridge[a]

[a]The indicated source of the plume is uncertain.
* Plumes with only one tracer recorded for the flight were not used for the tracer-tracer relationship analysis.
** Overlapping plumes with different particle to gas ratios.
*** Mean wind direction at the site was coming from the west (opposite from power plants' locations).

In Table S8 a question mark indicates that the source is unknown or uncertain. For two plumes, the recorded flight data was insufficient to perform an analysis of tracer ratios (rows in grey shading). These plumes were therefore not used in the analysis. On February 9, two plumes (plume ID 141 and 142) with distinct tracer ratios were observed at very similar heights and were partially overlapping. After careful comparison with FLEXPART-WRF model tracer results, plume 142 was attributed to UAF C as it showed similar ratios to those observed in other UAF C plumes. For plume 141, it is uncertain whether the observed peak belongs to plume 141 despite the vertical displacement or if the origin is different. According to the FLEXPART-WRF results, Zehnder could also be a potential source in this case. Given the slight overlap of these two plumes, their tracer ratios might therefore be different as a result of mixing of the different species. On February 23, a plume (ID 231) was observed at 50 m above ground with wind directions of 290°. Given the wind direction, a likely source could be located on Chena ridge (Fig. 1).